Journal Name

Dynamic Article Links ►

Cite this: DOI: 10.1039/c0xx00000x

www.rsc.org/xxxxxx

ARTICLE TYPE

Rod-like mesoporous silica nanoparticles with rough surfaces for enhanced cellular delivery

Chun Xu, Yuting Niu, Amirali Popat, Siddharth Jambhrunkar, Surajit Karmakar and Chengzhong Yu*

Received (in XXX, XXX) Xth XXXXXXXXX 20XX, Accepted Xth XXXXXXXXX 20XX

DOI: 10.1039/b000000x

Novel rod-like mesoporous silica nanoparticles with a rough surface have been prepared with 37% higher cellular uptake and drug delivery efficacy compared to their counterpart with a smooth surface.

Delivery of various drugs into target cells is crucial in modern medicine.[1, 2] Some free drugs, e.g. hydrophobic molecules, are poorly delivered to the cells due to intrinsic issues such as low solubility and/or unwanted toxicity.[1] To circumvent these problems, various nanoparticle based drug delivery systems (DDS), prepared by liposomes, lactic acid, peptide, chitosan, polymers, carbon, silica, *etc*,[1-3] have been developed. The positive effect of DDS on the stability of drugs has also been demonstrated.[4] Among them, mesoporous silica nanoparticles (MSN) have attracted great attention[5] due to their unique features including good biocompatibility,[6, 7] ordered pore network,[8, 9] tunable surface chemistry,[10] and high drug loading capacity.[9, 11] Many studies focused on the impacts of particles size,[12-14] shape,[15-18] surface chemical modification[10, 19] on the cellular uptake and delivery performance. Bare silica has relatively low cellular uptake capability, hence surface functionalization of MSN with positively charged groups such as amine group,[19, 20] poly ethylene imine (PEI)[21] and poly-L-lysine (PLL)[22] have been studied to enhance the interaction with negatively charged cell membranes. However, MSN after functionalization are generally toxic, limiting their use in the clinical setting. It remains a challenge to further improve the delivery efficiency of MSN with a pure silica composition. [23]

The rapid development of bio-inspired and bio-mimetic chemistry has provided new approaches for the rational design of functional nanomaterials with enhanced performance. In nature, after millions of years' evolution, viruses have developed very efficient ways to enter cells. For example, virus in *Rhabdoviridae* family with characteristic rod-like shape can infect a broad range of hosts including humans.[24] It is noted that rod-like MSN have been studied as nano-carriers with excellent cellular uptake efficacy.[16, 17, 25] On the other hand, most viruses including rhabdovirus have rough surface with spikes located on the outer membranes.[24] Previous studies[26-28] have successfully proved that nano-scale surface roughness enhances the cellular uptake of solid nanoparticles. However, there is no report to apply this concept in the synthesis of MSNs to improve the cellular uptake and drug delivery performance.

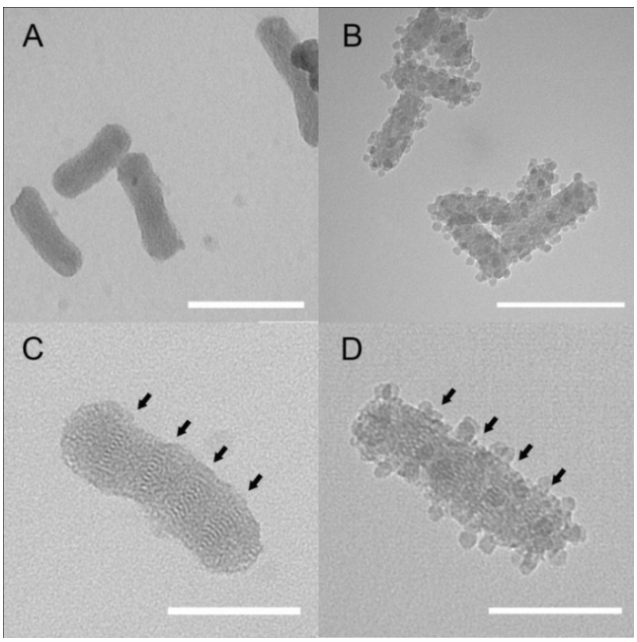

Fig. 1 TEM images of R-MCM-41(A, C) and RR-MCM-41(B, D). The fringes indicated by dark arrows correspond to (10) plane of the hexagonal structure. Scale bar in A, B: 200 nm; scale bar in C, D: 100nm.

In this communication, we report the synthesis and cellular delivery performance of novel rod-like MSN with a rough surface. MCM-41 type MSN with a rod-like morphology (denoted R-MCM-41) were prepared using our reported protocol[29] (see †ESI), using cetyltrimethylammonium bromide and perfluorooctanoic acid as co-templated and tetraethyl orthosilicate as the silica source. The as-synthesised products were functionalized with amino group, followed by conjugation with negatively charged silica shell particles with small size (~13nm) prepared by a modified Stöber method,[30] forming rough R-MCM-41 (denoted RR-MCM-41). The final products were calcined at 550 °C for both R-MCM-41 and RR-MCM-41, ensuring that the two materials under study have the same pure silica composition.

Figure 1 shows the transmission electron microscopy (TEM) images of both R-MCM-41 (Fig. 1A&C) and RR-MCM-41(Fig

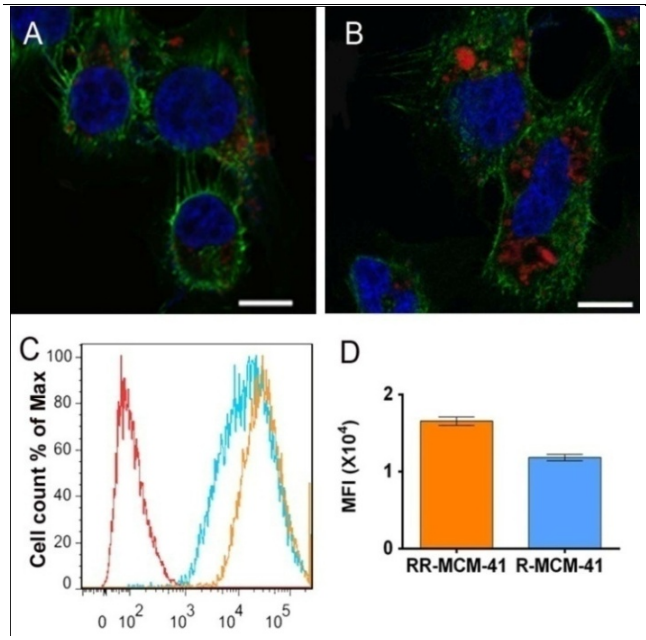

Fig. 2 Cellular uptake of R-MCM-41 and RR-MCM-41. Confocal microscopy images (A & B) show the localisation of RITC (red color) in KHOS cell line delivered by R-MCM-41(A) and RR-MCM-41(B). The nuclei are stained in blue (DAPI) and the cytoplasm in green (FITC).FACS analysis (C) and comparison of the normalised MFI (D) indicate that RR-MCM-41-FITC has higher cellular uptake efficiency than R-MCM-41-FITC after 4h. Scale bar in A, B: 10μm.

.1B&D). R-MCM-41 possesses a rod-like morphology with an average aspect ratio of 3:1 (Fig. 1A). The fringes indicated by the dark arrows in Fig. 1C correspond to (10) plane of hexagonal structure, in accordance with our previous report.[29] The rod-like morphology is retained in RR-MCM-41, while the outer surface is uniformly coated by small silica spheres (Fig. 1B&D). The (10) fringes can also be observed as indicated by the black arrows in RR-MCM-41 (Fig. 1D).

The small angle X-ray diffraction pattern of R-MCM-41 (Fig. S1A, †ESI) shows three well-resolved peaks at 2θ of 2.35, 4.08 and 4.70° , which can be indexed as the 10, 11, and 20 reflections based on a two-dimensional hexagonal symmetry (*p6mm*). For RR-MCM-41, three diffractions are also observed but the intensity is much weaker compared to R-MCM-41 due to the existence of shell particles on the surface. Nitrogen adsorption-desorption measurements (Fig. S1B, Tab. S1) show that the RR-MCM-41 has a decreased BET surface area (613 m^2/g) compared to R-MCM-41 (703 m^2/g) because the shell particles are solid and have comparatively lower surface area than R-MCM-41. An increase in the total pore volume is observed for RR-MCM-41 (0.85 cm^3/g) compared to R-MCM-41 (0.59 cm^3/g), which is mainly contributed by the inter-particles packing voids as shown in the capillary condensation step at the relative pressure (P/P_0) higher than 0.9. The pore size of RR-MCM-41 is calculated to be 2.5 nm (Fig. S1C), slightly larger than R-MCM-41 (2.2 nm), which is caused by the hydrothermal treatment during the amino group modification step.

To compare the cellular uptake efficiency, R-MCM-41 and RR-MCM-41 were both labelled with a red fluorescent dye, Rhodamine B isothiocyanate (RITC), or with another green fluorescent dye, fluorescein 5(6)-isothiocyanate dye (FITC),

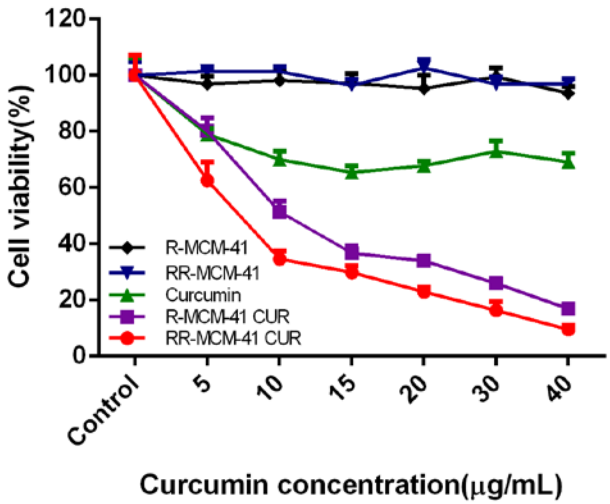

Fig. 3 ***In Vitro*** **cytotoxicity of R-MCM-41 CUR and RR-MCM-41 CUR in KHOS cell line after 24h incubation.**

using post-synthesis grafting methods (†ESI). The dye conjugated particles were incubated with KHOS, a human osteosarcoma cell line for 4 h. Confocal microscopy images (Fig. 3A, B) show that in either RITC (Fig. 2A&B) or FITC conjugated systems (Fig. S2) fluorescent signals with higher intensity are observed in RR-MCM-41 group compared to R-MCM-41, indicating that the rough particles have improved cellular uptake performance.

To quantitatively evaluate the cellular uptake efficiency of these two particles, fluorescence-activated cell sorting (FACS) analysis were used and median fluorescence intensity (MFI) were adopted to reflect the relative amount of internalized particles. MSN modified with FITC are used in this study and the grafting FTIC amount in both R-MCM-41 and RR-MCM-41 were tested to normalize MFI (Table. S2, †ESI). It is shown that RR-MCM-41 exhibits 37% higher cellular uptake efficiency than R-MCM-41 (Fig. 3C, D), in accordance with the confocal microscopy studies.

To compare the performance of R-MCM-41 and RR-MCM-41 as effective drug carriers, a hydrophobic drug, curcumin, is loaded into both particles by rotary evaporation method (see †ESI). From the thermogravimetric analysis (Fig. S3), it shows that the weight percentage of curcumin is 29.0% and 25.7% for RR-MCM-41 and R-MCM-41, respectively.

To confirm whether the drug molecules are loaded inside the pores, Fourier transform infrared spectroscopy (FTIR) and differential scanning calorimetry (DSC) technique is employed. As shown in Fig. S4, the peaks in the area of 1450-1630 cm^{-1} in R-MCM-41 CUR and RR-MCM-41 CUR come from the C=O and C=C group of curcumin. For DSC results (Fig. S5), pure curcumin (CUR) shows a sharp peak at 176 °C attributed to the phase transition from gel to liquid crystalline state.[31] Similar peak can be observed in the physical mixture of curcumin and R-MCM-41 samples. The peak intensity is weak due to the smaller amount of curcumin. However, in the curcumin loaded R-MCM-41(R-MCM-41 CUR) and RR-MCM-41 (RR-MCM-41 CUR), no peak around the melting temperature can be found, suggesting that curcumin has been loaded inside the pores. This can be further confirmed by the the anti-proliferative effects of R-MCM-

41 CUR and RR MCM-41 CUR are tested in KHOS cell line by MTT assay. As shown in Fig. 3, both R-MCM-41 and RR-MCM-41 themselves have no obvious toxicity to the cells at measured concentration range (0 -160 μg/mL). The pure curcumin kills less than 40% of the cells at the concentration of 15μg/mL, and no further cell death is observed at higher concentrations. The relatively low cell cytotoxicity of curcumin is associated with its low solubility and bioavailability. In contrast, R-MCM-41 CUR and RR-MCM-41 CUR caused significantly higher cell death compared to free CUR, for example at a curcumin concentration of 10 ug/mL, free CUR shows cell viability of 70% while R-MCM-41 CUR and RR-MCM-41 CUR show cell viability of 50% and 35%, respectively. Importantly, RR-MCM-41-CUR shows better cell cytotoxicity than R-MCM-41 CUR at all concentration tested. The IC50 value (inhibitory concentration necessary to inhibit 50% of cell growth) of R-MCM-41 CUR and RR-MCM-41 CUR are 11 μg/mL and 8 μg/mL, respectively. The IC 50 value of RR-MCM-41 CUR is around 37% lower than that of the R-MCM-41 CUR, consistent with the cellular entry results. Our results indicate that the enhanced cell toxicity of RR-MCM-41 CUR is associated with its higher cellular uptake performance, a result of rough surface modification in comparison with R-MCM-41 CUR.

In summary, a new approach to increase the cellular uptake and drug delivery performance of MSN with a pure silica composition has been demonstrated by introducing nano-scale surface roughness. Rod-like MSN with rough surface show superior cellular uptake efficacy than traditional MSN with smooth surface, and this is further confirmed by the higher cell toxicity induced by particles loaded with curcumin. Compared to literature reports, it is a big step moving from solid nanoparticles to MSN due to their intrinsic nanoporous properties, which are more suitable for drug delivery applications as demonstrated in this work. Our work on the contribution of nanoscale surface roughness in MSN systems will lead to a series of DDS with improved performance for drug delivery.

The authors acknowledge the support by Australian Research Council, Queensland Cancer Council and Queensland Government for financial supports. We thank the facilities of Australian Microscopy and Microanalysis Research Facility at the Centre for Microscopy and Microanalysis, the University of Queensland.

Notes and references

Australian Institute for Bioengineering and Nanotechnology, the Univesity of Queensland, Brisbane, QLD 4067, Australian. Fax:+61-7-334 63973; Tel:+61-7-334 63283; E-mail: c.yu@uq.edu.au

† Electronic Supplementary Information (ESI) available: sample preparation, small-angle XRD patterns, nitrogen adsorption-desorption isotherms and releated pore size distribution, confocal microscopy, TGA, DSC. See DOI: 10.1039/b000000x/

1. J. W. Yoo, D. J. Irvine, D. E. Discher and S. Mitragotri, *Nat. Rev. Drug. Discov.*, 2011, **10**, 521-535.

2. N. Niu, A. Popatt, M. Yu, S. Karmakar, W. Gu and C. Yu, *Therapeutic delivery*, 2012, **3**, 1217-1237.

3. R. A. Petros and J. M. DeSimone, *Nat. Rev. Drug. Discov.*, 2010, **9**, 615-627.

4. Maria Eugenia Carlotti, Simona Sapino, Elena Peira, Marina Gallarate and E. Ugazio, J. Disp. Sci. Technol, 2009, 30, 1517-1524.

5. M. Vallet-Regi, A. Ramila, R. P. del Real and J. Perez-Pariente, *Chem. Mater.*, 2001, **13**, 308-311.

6. M. H. Yu, S. Jambhrunkar, P. Thorn, J. Z. Chen, W. Y. Gu and C. Z. Yu, *Nanoscale*, 2013, **5**, 178-183.

7. J. Lu, M. Liong, Z. X. Li, J. I. Zink and F. Tamanoi, *Small*, 2010, **6**, 1794-1805.

8. S. B. Wang, *Micropor. Mesopor. Mat.*, 2009, **117**, 1-9.

9. M. Vallet-Regi, F. Balas and D. Arcos, *Angew. Chem. Int. Edit.*, 2007, **46**, 7548-7558.

10. I. Slowing, B. G. Trewyn and V. S. Y. Lin, *J. Am. Chem. Soc.*, 2006, **128**, 14792-14793.

11. S. Simovic and D. Losic, *Nanotechnol. Sci. Tech.*, 2010, 73-161.

12. Y. S. Lin, C. L. Haynes, *J. Am. Chem. Soc.*, 2010, **132**, 4834-4842.

13. Q. Gan, D. W. Dai, Y. Yuan, J. C. Qian, S. Sha, J. L. Shi and C. S. Liu, *Biomed. Microdevices.*, 2012, **14**, 259-270.

14. M. Ekkapongpisit, A. Giovia, C. Follo, G. Caputo and C. Isidoro, *Int. J. Nanomed.*, 2012, **7**, 4147-4158.

15. N. J. Hao, L. L. Li, Q. Zhang, X. L. Huang, X. W. Meng, Y. Q. Zhang, D. Chen, F. Q. Tang and L. F. Li, *Micropor. Mesopor. Mat.*, 2012, **162**, 14-23.

16. X. L. Huang, L. L. Li, T. L. Liu, N. J. Hao, H. Y. Liu, D. Chen and F. Q. Tang, *Acs. Nano.*, 2011, **5**, 5390-5399.

17. X. L. Huang, X. Teng, D. Chen, F. Q. Tang and J. Q. He, *Biomaterials*, 2010, **31**, 438-448.

18. T. Yu, A. Malugin and H. Ghandehari, *Acs. Nano.*, 2011, **5**, 5717-5728.

19. M. Manzano, V. Aina, C. O. Arean, F. Balas, V. Cauda, M. Colilla, M. R. Delgado and M. Vallet-Regi, *Chem. Eng. J.*, 2008, **137**, 30-37.

20. G. Berlier, L. Gastaldi, S. Sapino, I. Miletto, E. Bottinelli, D. Chirio and E. Ugazio, *Int. J. Pharm.*, 2013, **26**, 177-186.

21. T. A. Xia, M. Kovochich, M. Liong, H. Meng, S. Kabehie, S. George, J. I. Zink and A. E. Nel, *Acs. Nano.*, 2009, **3**, 3273-3286.

22. S. B. Hartono, W. Y. Gu, F. Kleitz, J. Liu, L. Z. He, A. P. J. Middelberg, C. Z. Yu, G. Q. Lu and S. Z. Qiao, *Acs. Nano.*, 2012, **6**, 2104-2117.

23. D. A. Jackson, S. Juranek, H. J. Lipps, *Mol. Ther*, 2006, **14**, 613-626.

24. J. H. Strauss and E. G. Strauss, *Viruses and Human Disease*, 2 edn., 2007.

25. D. Sen Karaman, D. Desai, R. Senthilkumar, E. M. Johansson, N. Ratts, M. Oden, J. E. Eriksson, C. Sahlgren, D. M. Toivola and J. M. Rosenholm, *Nanoscale. Res. Lett.*, 2012, **7**.

26. Y. Niu, M. Yu, S. B. Hartono, J. Yang, H. Xu, H. Zhang, J. Zhang, J. Zou, A. Dexter, W. Gu and C. Yu, *Adv. Mater.*, 2013.

27. M. Massignani, C. LoPresti, A. Blanazs, J. Madsen, S. P. Armes, A. L. Lewis and G. Battaglia, *Small*, 2009, **5**, 2424-2432.

28. C. LoPresti, M. Massignani, C. Fernyhough, A. Blanazs, A. J. Ryan, J. Madsen, N. J. Warren, S. P. Armes, A. L. Lewis, S. Chirasatitsin, A. J. Engler and G. Battaglia, *Acs. Nano.*, 2011, **5**, 1775-1784.

29. S. Yang, L. Zhao, C. Yu, X. Zhou, J. Tang, P. Yuan, D. Chen and D. Zhao, *J. Am. Chem. Soc.*, 2006, **128**, 10460-10466.

30. T. Yokoi, Y. Sakamoto, O. Terasaki, Y. Kubota, T. Okubo and T. Tatsumi, *J. Am. Chem. Soc.*, 2006, **128**, 13664-13665.

31. K. Maiti, K. Mukherjee, A. Gantait, B. P. Saha and P. K. Mukherjee, *Int. J. Pharm.*, 2007, **330**, 155-163.